



This article appeared in a journal published by Elsevier. The attached copy is furnished to the author for internal non-commercial research and education use, including for instruction at the authors institution and sharing with colleagues.

Other uses, including reproduction and distribution, or selling or licensing copies, or posting to personal, institutional or third party websites are prohibited.

In most cases authors are permitted to post their version of the article (e.g. in Word or Tex form) to their personal website or institutional repository. Authors requiring further information regarding Elsevier's archiving and manuscript policies are encouraged to visit:

<http://www.elsevier.com/copyright>



Contents lists available at SciVerse ScienceDirect

# Journal of Quantitative Spectroscopy & Radiative Transfer

journal homepage: [www.elsevier.com/locate/jqsrt](http://www.elsevier.com/locate/jqsrt)

## Discrete dipole approximation for low-energy photoelectron emission from NaCl nanoparticles

Matthew J. Berg<sup>a,\*</sup>, Kevin R. Wilson<sup>b</sup>, Christopher M. Sorensen<sup>c</sup>,  
Amit Chakrabarti<sup>c</sup>, Musahid Ahmed<sup>b</sup>

<sup>a</sup> Department of Physics & Astronomy, Mississippi State University, Mississippi State, MS 39762, USA

<sup>b</sup> Chemical Sciences Division, Lawrence Berkeley National Laboratory, Berkeley, CA 94720, USA

<sup>c</sup> Department of Physics, Kansas State University, Manhattan, KS 66506, USA

### ARTICLE INFO

#### Article history:

Received 10 August 2011

Received in revised form

13 October 2011

Accepted 14 October 2011

Available online 19 October 2011

#### Keywords:

Electromagnetic scattering

Internal field

Photoemission

Nanoparticle

Nonspherical particle

Discrete dipole approximation

### ABSTRACT

This work presents a model for the photoemission of electrons from sodium chloride nanoparticles 50–500 nm in size, illuminated by vacuum ultraviolet light with energy ranging from 9.4 to 10.9 eV. The discrete dipole approximation is used to calculate the electromagnetic field inside the particles, from which the two-dimensional angular distribution of emitted electrons is simulated. The emission is found to favor the particle's geometrically illuminated side, and this asymmetry is compared to previous measurements performed at the Lawrence Berkeley National Laboratory. By modeling the nanoparticles as spheres, the Berkeley group is able to semi-quantitatively account for the observed asymmetry. Here however, the particles are modeled as cubes, which are closer to their actual shape, and the interaction of an emitted electron with the particle surface is also considered. The end result shows that the modeled emission asymmetry for these low-energy electrons is more sensitive to the interaction with the particle-surface than to the specific particle shape, i.e., a sphere or cube.

© 2011 Elsevier Ltd. All rights reserved.

### 1. Introduction

The interaction of ionizing radiation with nanoparticles is important to understanding a variety of phenomena ranging from atmospheric nucleation to the heating of dust clouds by secondary electron emission from interstellar grains [1,2]. Photoelectron emission (PE) is currently being used as an analytical probe of soot formation within flames [3,4], for the detection of diesel emission [5], as spectroscopic probes of micron-sized droplet surfaces [6], sub-nanometer particles, and bio-aerosols [7]. A number of fundamental studies of nanoparticles, 5–200 nm in size,

have revealed both unexpectedly large PE quantum yields [8] and circular dichroism [9], the magnitude of which depends upon particle size. In many of these studies, the role that particle size and shape plays in both the electromagnetic absorption and PE remains an active area of research.

In a recent publication [10], Wilson et al. measure the two-dimensional angular distributions of photoelectrons emitted from sodium chloride (NaCl) nanoparticles exposed to vacuum ultraviolet (VUV) light at various photon energies around 10 eV. The key finding is an asymmetry in the angular PE distribution. At photon energies where the electromagnetic absorption length in the NaCl material is on the order of, the nanoparticle size, emission is observed preferentially from the geometrically illuminated side of the particle relative to the shaded side. Moreover, this asymmetry is inversely proportional to the particle size.

\* Corresponding author. Tel.: +1 785 317 3378;

fax: +1 662 325 8898.

E-mail address: [mberg81@gmail.com](mailto:mberg81@gmail.com) (M.J. Berg).

To investigate the cause and possible utility of this asymmetry, Wilson et al. employ a model of the emission process in which the particles are approximated as spheres and the PE trajectory within the particle is treated ballistically. Approximating the particles as spheres allows Mie theory to be used to calculate the internal (VUV) field from which emission is initiated. This model is able to reproduce the general trend of the observed PE asymmetry, implying that the asymmetry is due to the nonuniform illumination of the particle's interior caused by electromagnetic absorption. However, the agreement between the measured and modeled asymmetry is loose enough to suggest that a more sophisticated treatment could better fit the measurements. The following will describe such a model and compare its results to those reported by Wilson et al. More broadly, the following work demonstrates the application of a versatile electromagnetic-scattering model to a unique problem in nanoparticle science.

## 2. Model description

In the measurements [10], VUV light produced by the Advanced Light Source synchrotron at the Lawrence Berkeley National Laboratory is used to illuminate a stream of size-selected NaCl nanoparticles. The range of photon energies used include 9.4, 10.0, and 10.9 eV, which exceeds the NaCl ionization threshold [11] of  $8.2 \pm 0.1$  eV, and the nanoparticle sizes range from approximately 50 to 500 nm. To acquire two-dimensional angular PE images, electrostatic lenses focus photoelectrons onto a dual multichannel-plate coupled to a phosphor screen, imaged onto a charged coupled device (CCD) camera. The resulting digital image is then numerically analyzed to infer the emission asymmetry.

The new model developed here begins with a representation of the nanoparticle shape. Fig. 1(a) shows scanning electron microscope (SEM) images of the types of nanoparticles used in the measurements. These particles are cube-like with rounded edges and some sign of either surface roughness and/or internal inhomogeneity. As an approximation, a homogeneous cube of length  $L$  is

taken to represent a particle, see Fig. 1(b). Spherical model-particles will also be used to understand the effect of particle morphology on the PE emission. In the measurements, each particle enters the VUV beam in a random orientation, which is described in the model using two coordinate systems called the laboratory and particle-systems,  $(x_L, y_L, z_L)$  and  $(x_P, y_P, z_P)$ , respectively. These systems share a common origin at the particle center, and the  $z$ -axis of the laboratory system is taken along the propagation direction of the VUV beam.

The electric field of the VUV light, which will be called the incident field  $E^{\text{inc}}$ , is taken to be a linearly polarized plane wave

$$E^{\text{inc}}(\mathbf{r}) = E_0 \exp(ik\hat{\mathbf{n}}^{\text{inc}} \cdot \mathbf{r}), \quad (1)$$

where  $\hat{\mathbf{n}}^{\text{inc}}$  describes the propagation direction, and  $E_0$  is a constant proportional to the light intensity. Meanwhile, the  $x_L$  and  $y_L$ -axes are taken along the particle-beam direction, and the direction from the origin to the detector, respectively, refer to Fig. 1(b).

The relative orientation of the two coordinate systems is described by the Euler rotation angles  $(\alpha, \beta, \gamma)$ ; transformation between the systems is accomplished by a rotation matrix and its inverse [12]. A random particle-orientation can be realized by choosing three random numbers  $\{x_1, x_2, x_3\}$  in the interval  $[0, 1]$  from which the Euler angles are calculated as

$$\alpha = 2\pi x_1, \quad \beta = \cos^{-1}(2x_2 - 1), \quad \gamma = 2\pi x_3. \quad (2)$$

Defining  $N_{\text{ori}}$  sets of Euler angles this way results in a collection of as many particle orientations sampled randomly from all directions [13]. The number of orientations used in each simulation below is determined by observing the convergence of the asymmetry parameter (Section 3) with varying  $N_{\text{ori}}$ ; in most cases a total of ten orientations is sufficient.

Next, the electric field  $E^{\text{int}}$  inside the particle is found for each orientation. This is done using the Discrete Dipole Approximation (DDA), which in essence is a numerically exact way to solve the Maxwell equations for any particle [14]. To implement the DDA however, requires knowledge of the nanoparticle refractive index  $m$ , which is estimated [15] to be  $m = 1.79 + 0.55i$  for a photon energy of 9.4 eV,

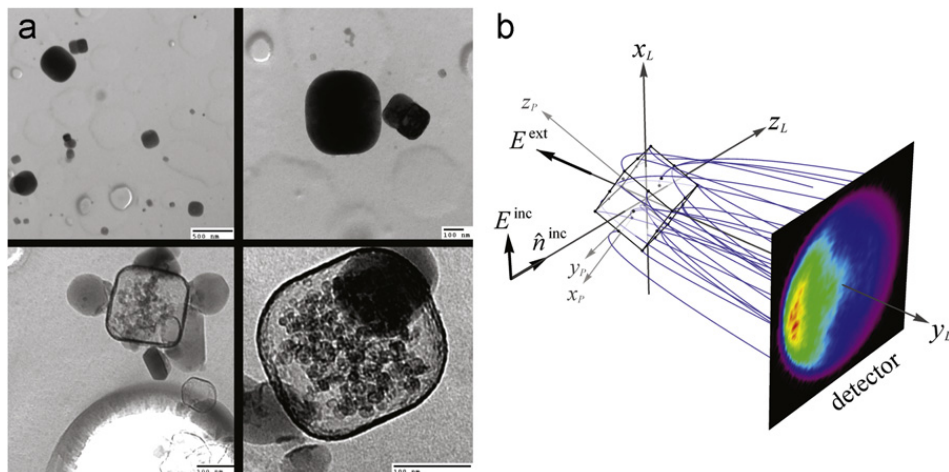


Fig. 1. SEM images (a) of the NaCl nanoparticles used by Wilson et al., and a diagram (b) of the modeled emission process.

$m=1.7+0.64i$  for 10.0 eV, and  $m=2.15+0.60i$  for 10.9 eV. The “approximation” in the DDA is that the particle is represented by a collection of coupled electric-dipoles that reside on a cubic lattice spanning the particle volume. Thus, the accuracy of the calculation is determined by the fineness of this lattice. Typically, one uses a lattice spacing that is roughly  $\lambda'/10$ , where  $\lambda'$  is the wavelength in the particle material [14]. Given the photon energies considered and associated refractive indexes, the smallest refracted wavelength is  $\lambda'=52$  nm, and hence a lattice spacing corresponding to  $l=5$  nm is used.

The DDA program used here is a custom-made suite of code developed by the authors. Although there are several excellent open-source codes available, such as the so-called Amsterdam-DDA developed by Yurkin and Hoekstra, a custom-made implementation is more easily incorporated within the photoelectron emission model. For verification purposes, the scattered electric field provided by the simulations for homogeneous spheres and spheroids of various sizes, refractive indexes, and orientations is compared to the exact field provided by Mie theory (for spheres) and the widely used T-Matrix code of Mishchenko (for spheroids) [12]. The results of this comparison show agreement between the DDA and the exact calculations to within 1–5%, on average for the particles considered. Different implementations of the DDA use varying techniques to relate the particle refractive index to each dipole's polarizability; the one used here is the so-called Lattice Dispersion Relation (LDR), which is chosen because of its apparent wide use and accurate results yielded during the verification study. The dipole lattice spacing of  $\lambda'/10$  and use of the LDR are parameters of the DDA model known to affect its accuracy, and are found to be satisfactory for the purposes of this work. For example, no convergence failures occurred with the code when applied across the particle size-range

considered. However, the results of this work should not be regarded as a rigorous study of the convergence of the DDA for particle internal-fields.

Other techniques to find the electromagnetic field in nonspherical particles are available. However, the DDA is well-suited for this application because the shape of the model particle exactly coincides with the dipole lattice geometry; hence, there are no so-called shape errors that can sometimes degrade the accuracy of DDA simulations of nonspherical particles, e.g., see [14]. The sharp corners and edges of the particle, which typically cause enhancements in the internal-field magnitude, are also not problematic in these DDA calculations. Fig. 2 shows an example of the surface-field magnitude for two cubic particles, one with and one without absorption. The absorbent particle corresponds to a size and refractive index consistent with those in the measurements.

Once  $\mathbf{E}^{\text{int}}$  is known at each lattice site  $\mathbf{r}_s$  in the particle, the PE can be simulated. This process is in-part based on Wilson et al. and includes the following steps that are performed at each site for each particle orientation:

- (1) A random direction  $\hat{\mathbf{r}}_e$  for electron emission is chosen following Eq. (2) and is represented by the corresponding Euler angles  $\{\alpha_e, \beta_e, \gamma_e\}$ .
- (2) The straight-line distance  $d$  from  $\mathbf{r}_s$  to the particle surface along the direction  $\hat{\mathbf{r}}_e$  is found.
- (3) An emission probability  $P$  is then assigned to this electron according to the equation:

$$P = c |\mathbf{E}^{\text{int}}|^2 \sin \theta \sin^2 \delta e^{-d/r_{\text{mfp}}} \quad (3)$$

where  $\theta$  is the polar angle in the laboratory frame, i.e., the angle between  $\hat{\mathbf{r}}_e$  and  $\hat{\mathbf{n}}^{\text{inc}}$ ,  $\delta$  is the angle between  $\hat{\mathbf{r}}_e$  and  $\mathbf{E}^{\text{int}}$  at the site,  $r_{\text{mfp}}$  is the electron mean free path, and  $c$  is a normalization factor.

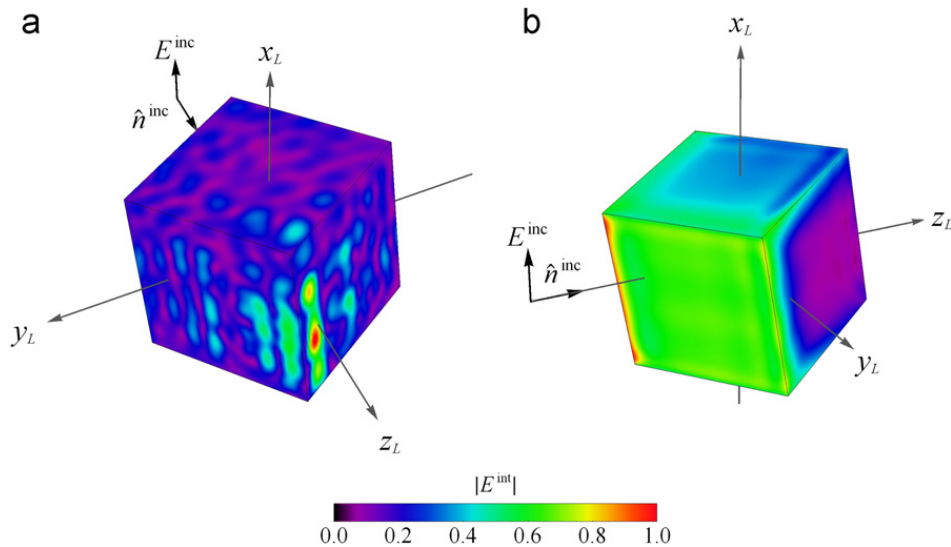


**Fig. 2.** Examples of the electric field magnitude at the surface of a cubic nanoparticle calculated with DDA. The particle in (a) has refractive index  $m=1.79+0i$  and hence is nonabsorbent, unlike the particles in the measurements and the one shown in (b) where  $m=1.79+0.55i$ . Comparison between the two shows that an enhancement in the field occurs on the side of the nonabsorbent particle where the incident light leaves it, i.e., along the positive  $z_L$ -axis. This is an example of a so-called hot spot, which does not occur for the absorbent particle. Rather, the large field magnitude for the absorbing particles occurs along the edges and corners of the geometrically illuminated side, which can be seen in (b). Note that the perspective of the two particle is different; particle back-side view in (a) and particle-side view in (b). The size parameter of both particles is  $kR=10.4$  where  $\lambda=131.9$  nm and the number of dipoles used in the calculation to represent a cube is  $N=216,000$ .



- (4) The angle between the particle-surface normal  $\hat{n}$  and  $\hat{r}_e$  at the point where the (linear) electron trajectory intersects the particle surface is found. This angle, denoted  $\xi$  is compared to the so-called escape-cone angle  $\theta_{\text{esc}}$ ; if  $\xi \leq \theta_{\text{esc}}$  then the electron is counted as leaving the particle, but is not if  $\xi > \theta_{\text{esc}}$ .

Fig. 3 shows a sketch illustrating the angles and vectors involved in this emission process. The factor of  $\sin\theta$  in

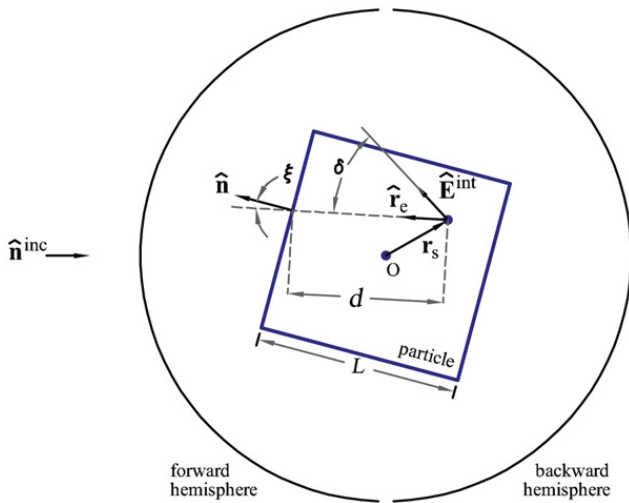


**Fig. 3.** Diagram showing a particle along with the vectors and angles used to model the emission process. Also indicated is the propagation direction of the VUV light  $\hat{n}^{\text{inc}}$ , and the forward and backward hemispheres used to calculate the PE asymmetry parameter  $\alpha$  described below.

Eq. (3) accounts for the weighting associated with integration over the polar angle, while the factor  $\sin^2\delta$  accounts for the angular dependence of PE from a lattice site assuming dipole excitation [10]. The inclusion of the escape-cone angle was not implemented in the Wilson et al. model. Use of this angle to restrict which electron trajectories contribute to particle ionization has been proposed before [16], but has not been implemented in a sophisticated model like is done here. In short, this angle requires that an electron overcome an electrostatic image-based surface potential before it is permitted to completely leave the particle. One will see below that this angle significantly affects the emission asymmetry  $\alpha$ .

Once an electron has left the particle, it is accelerated to the detector plane by an external static field  $E^{\text{ext}}$ , and examples of the resulting parabolic electron trajectories are shown in Fig. 1(b). To simulate the measured detector-images, this plane is divided into an array of  $64 \times 64$  pixels. The probability  $P$  given to each electron in step (2) is then assigned to the pixel within which it intercepts the plane. If more than one electron intercepts a given pixel, the associated probabilities are added, then the entire array is normalized by the largest pixel value after all particle orientations have been considered. The resulting distribution tends to be disk-like in shape due to the multiple particle-orientations used and this is seen in Fig. 4 below.

### 3. Emission asymmetry

Fig. 4 shows a comparison of the measured (left) and modeled (right) two-dimensional angular PE images at

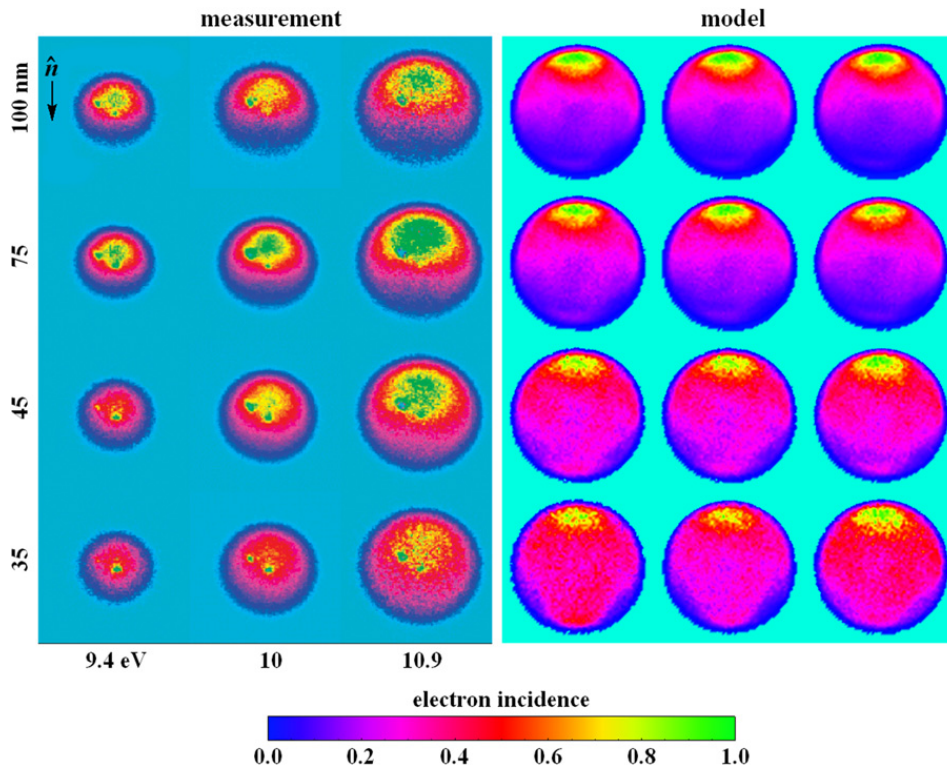


**Fig. 4.** Measured and modeled two-dimensional angular PE images. The propagation direction of the VUV light is indicated by the arrow in the top left, recall Figs. 1(b) and 3. The particle equivalent-sphere radii and photon energy labeled on the measured images also apply to the modeled ones.

various photon energies across a distribution of particle sizes. In the measurements, the size is described in terms of the radius  $R$  of a sphere that just fits inside a cube of length  $L$ , i.e.,  $R=L/2$ . For the model, the electron mean free path and escape-cone angle are  $r_{\text{mfp}}=10.0$  nm and  $\theta_{\text{esc}}=\pi/4$ , respectively. Note that as discussed at the end of this section, this choice for  $r_{\text{mfp}}$  and  $\theta_{\text{esc}}$  gives results that best fit the measurements when a cube is used as the model particle. However, the value for  $\theta_{\text{esc}}$  giving an acceptable agreement with measurement is different if a spherical model-particle is used. One can see that the emission displays a pronounced asymmetry. More photoelectrons are emitted into the forward hemisphere, which consists of directions with negative projection along the  $z_L$ -axis, as compared to the backward hemisphere, i.e., emission directions with positive  $z_L$ -axis projections. The projection of these hemispheres onto the detector plane corresponds to the top and bottom half of the images. Qualitatively, the measured and modeled images agree reasonably well. One can see that there is more emission into the forward hemisphere, revealing that the emission originates more from the geometrically illuminated side

of a particle. The measurement images show regions of peak emission, i.e., yellow, over a larger extent of the image than do the model images. In the modeled images, the peak emission is localized more to the top of the image. A possible explanation for this apparent discrepancy is that the measured images shown are not corrected for variations in the particle positions within the VUV beam, whereas the particles in the model are always at the origin when emission is simulated. The consequence of varying particle-position in the measurement consisting of an ensemble of many individually illuminated particles can be to smear the angular structure of the net emission. Such a distortion of the PE distribution could account for the qualitative difference seen in Fig. 4.

To better quantify the emission asymmetry, the top and bottom halves of the detector images are integrated, and the ratio of the resulting values defines the asymmetry parameter  $\alpha$ . If  $\alpha=1$ , photoelectrons are emitted equally into the forward and backward hemispheres, whereas if  $\alpha < 1$  more electrons are emitted into the forward hemisphere relative to the backward hemisphere, recall Fig. 3. Fig. 5 presents a series of comparisons between the

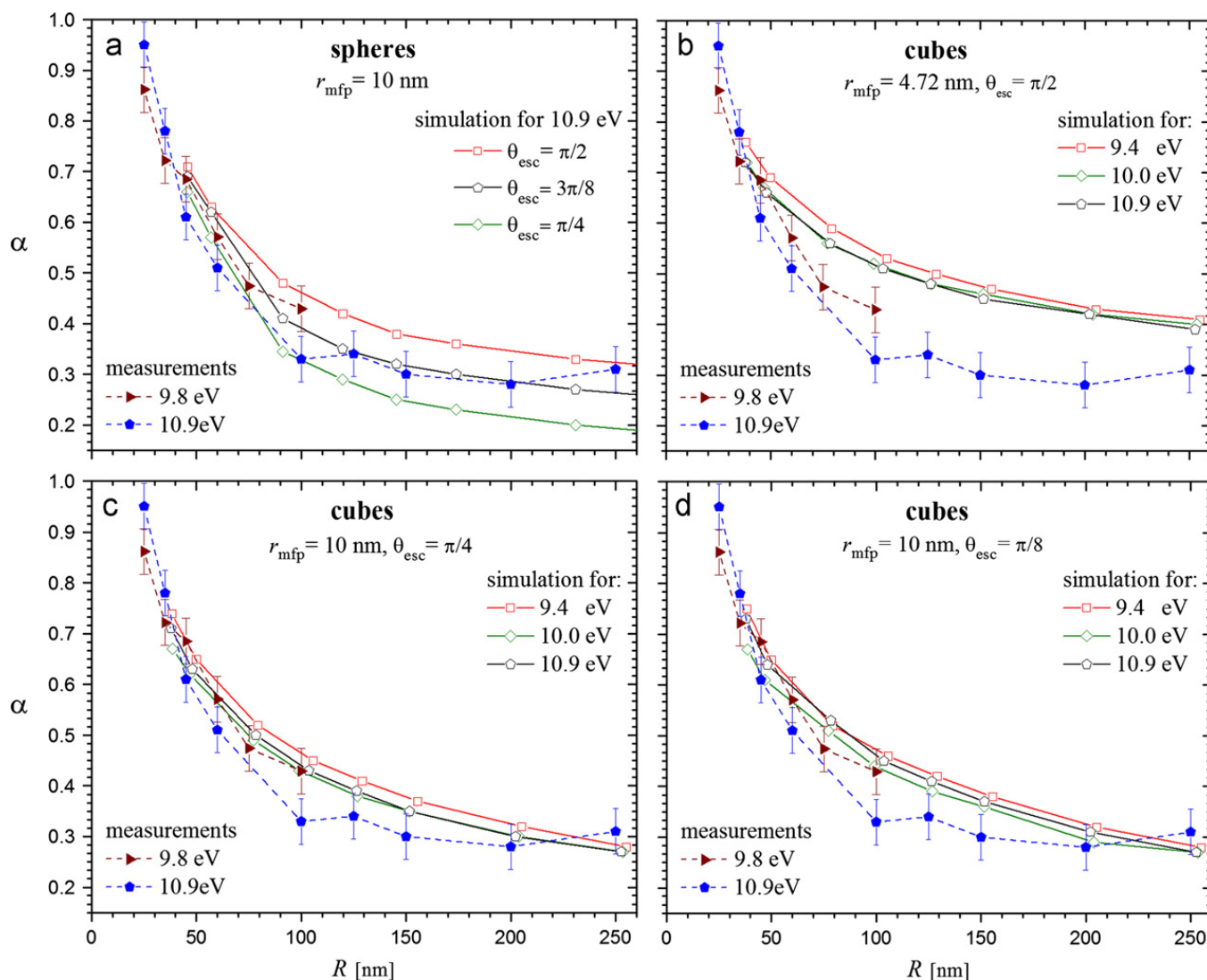


**Fig. 5.** Measured and modeled asymmetry-parameter  $\alpha$  curves as a function of particle radius  $R$  using spheres and cubes as the model-particle shape. The measured data is shown for 9.8 and 10.9 eV only, whereas the modeled curves are presented for the same energies as in Fig. 4.

measured  $\alpha$  as a function of equivalent-sphere particle size  $R$  for photon energies of 9.8 and 10.9 eV, and the modeled  $\alpha$  using either spheres or cubes. The rationale for considering a sphere as a model particle here is to connect with the work done by Wilson et al. This provides a degree of validation for the DDA-based model in addition to giving a sense of the effect that the model-particle shape has on  $\alpha$ .

The curves in Fig. 5(a) are generated using a sphere as the model particle, but otherwise following exactly the same procedure as described in Section 2. Here, the photon energy is 10.9 eV and the escape-cone angle is varied from  $\pi/2$  to  $3\pi/8$  to show how this parameter affects the asymmetry. Note that the curve for  $\theta_{\text{esc}} = \pi/2$  would correspond to the model curve presented by Wilson et al. The best agreement with the measurements is seen when  $\theta_{\text{esc}} = 3\pi/8$  and the electron mean free path is  $r_{\text{mfp}} = 10.0$  nm, the latter of which is consistent with Wilson et al. and expectations from the literature.

Fig. 5(b) through (d) use cubes as the model particles. In these plots, both  $r_{\text{mfp}}$  and  $\theta_{\text{esc}}$  are varied using three photon energies to investigate whether the more-realistic particle shape improves the agreement between the modeled and measured asymmetry. As with the spherical model-particle, the overall effect of decreasing the escape cone angle is to reduce the asymmetry  $\alpha$  and hence exaggerate the PE asymmetry. Moreover, this effect appears to be largely independent of the photon energy and mean free path; compare plots (c) and (d). Asymmetry curves generated using  $r_{\text{mfp}} = 10.0$  nm and  $\theta_{\text{esc}} = \pi/2$  appear nearly identical to those shown in Fig. 5(b) where  $r_{\text{mfp}} = 4.72$  nm, and hence are not shown here. This result is noteworthy however, since it shows that variation in the mean free path has less influence on  $\alpha$  than the escape-cone angle. The best agreement to the measurements occurs when  $\theta_{\text{esc}} = \pi/4$  and  $r_{\text{mfp}} = 10.0$  nm [plot (c)], although surprisingly, the agreement is not as good as that seen when a sphere is used as the model particle, i.e. plot (a). This suggests that for these photon energies, the particle shape has less influence on the emission asymmetry than the electron mean free path and escape-cone angle.

#### 4. Discussion

One question raised by Wilson et al. is whether the difference between the modeled and measured asymmetry is due to the approximation of the nanoparticle shape as a sphere or is due to the simple ballistic electron-transport model used. The results above suggest that for these photon energies approximations of the particle shape and electron transport have weaker influence on the asymmetry than accounting for an electron's interaction with the particle surface. From the point of view of the energies involved, this seems plausible: the photon energies are at most 2.7 eV above the ionization threshold of  $8.2 \pm 0.1$  eV for bulk NaCl [1,11]. Then, an electron liberated from a lattice site within the nanoparticle has low kinetic energy compared to this threshold as it emerges from the particle. Electrostatic image-forces may then significantly affect the electron's initial

trajectory. The escape-cone cutoff angle is, in a sense, a crude “first-order” way to build-in this interaction.

With regard to which model-particle shape is more appropriate, the results show that spheres fit the measurements slightly better than cubes, recall Fig. 5. One may find this surprising given that the crystal structure of NaCl is cubic. However, the SEM images of the particles in Fig. 1 reveal that the edges and corners of the cubic particles are rounded, more resembling a sphere-like shape in some cases. In addition, the measured PE images are the result of contributions from many randomly oriented particles. It is plausible then that much of the nonspherical-shape signatures in the angular emission distribution are washed out by the averaging over these orientations. In other words, one would expect to see much more structure in the PE image corresponding to a single particle measurement. Unfortunately, such measurements are not available for comparison, but with the development of ultrafast extreme-ultraviolet and X-ray lasers that can probe the electronic dynamics of single nanoparticles, new measurements relating to how particle shape couples with electron escape dynamics might be possible in the future. Lastly, one could propose further simulations using even more realistic particle shapes, such as a rounded cube. Indeed the DDA model can accommodate arbitrary particle shapes, and such improvements in the shape are a topic for future work. It is not clear, however, how this would improve the agreement between the modeled and measured asymmetry given that the electron transport is treated in such a simplistic manner; improvements in this regard are also topics for future study.

#### Acknowledgments

We thank the Kansas State University electron microscope facility for the SEM images of the NaCl particles used in this work. We also thank two anonymous reviewers for their helpful comments. This work was partly supported by the NASA Graduate Student Researchers Program. K.R. Wilson and M. Ahmed are supported by the Director, Office of Energy Research, Office of Basic Energy Sciences, Chemical Sciences Division of the US Department of Energy under Contract no. DE-AC02-05CH11231.

#### References

- [1] Wilson KR, Bluhm H, Ahmed M. Aerosol photoemission. In: Signorell R, Reid JP, editors. *Fundamentals and Applications in Aerosol Spectroscopy*. Boca Raton: CRC Press; 2010.
- [2] Draine BT. *Annual Review of Astronomy and Astrophysics* 2003;41: 241.
- [3] Mitchell JBA, Rebrion-Rowe C, Legarrec JL, Taupier G, Huby N. *Combustion and Flame* 2002;131:308.
- [4] Burtscher H, Schmidt-Ott A, Siegmund HC. *Aerosol Science and Technology* 1988;8:125.
- [5] Starr DE, Wong EK, Worsnop DR, Wilson KR, Bluhm H. *Physical Chemistry Chemical Physics* 2008;10:3093.
- [6] Grimm M, Langer B, Schlemmer S, Lischke T, Becker U, Widdra W, et al. *Physical Review Letters* 2006;96:1.
- [7] Wilson KR, Peterka DS, Jimenez-Cruz M, Leone SR, Ahmed M. *Physical Chemistry Chemical Physics* 2006;8:1884.

- [8] Schmidt-Ott A, Schurtenberger P, Siegmann HC. *Physical Review Letters* 1980;45:1284.
- [9] Kasper M, Keller A, Paul J, Siegmann K, Siegmann HC. *Journal of Electron Spectroscopy and Related Phenomena* 1999;98–99:83.
- [10] Wilson KR, Zou S, Shu J, Ruhl E, Leone SR, Schatz GC, et al. *Nano. Letters* 2007;7:2014.
- [11] Taylor JW, Hartman PL. *Physical Review* 1959;113:1421.
- [12] Mishchenko MI, Travis LD, Lacis AA. *Scattering, Absorption, and Emission of Light by Small Particles*. Cambridge: Cambridge University Press; 2002.
- [13] Morawiec A. *Orientations and Rotations*. Berlin: Springer; 2004.
- [14] Yurkin MA, Hoekstra AG. *Journal of Quantitative Spectroscopy and Radiative Transfer* 2007;106:558.
- [15] Miyata T, Tomiki T. *Journal of the Physical Society of Japan* 1968;24:1286.
- [16] Ferrini G, Michelato P, Parmigiani F. *Solid State Communications* 1998;106:21.